

Role of the Axial Base in the Modulation of the Cob(I)alamin Electronic Properties: Insight from QM/MM, DFT, and CASSCF Calculations

Neeraj Kumar,[†] Mercedes Alfonso-Prieto,^{‡,§} Carme Rovira,^{‡,||} Piotr Lodowski,[⊥] Maria Jaworska,[⊥] and Paweł M. Kozłowski^{*,†}

[†]Department of Chemistry, University of Louisville, Louisville, Kentucky 40292, United States

[‡]Institut de Química Teòrica i Computacional (IQT-CUB) and Computer Simulation and Modeling Laboratory (CoSMoLab), Parc Científic de Barcelona, Baldíri Reixac 10-12, 08028 Barcelona, Spain

[§]Institute for Computational Molecular Science, Temple University, 1900 North 12th Street, Philadelphia, Pennsylvania 19122, United States

^{||}Institució Catalana de Recerca i Estudis Avançats (ICREA)

[⊥]Department of Theoretical Chemistry, Institute of Chemistry, University of Silesia, Szkolna 9, PL-40 006 Katowice, Poland

 Supporting Information

ABSTRACT: Quantum chemical computations are used to study the electronic and structural properties of the cob(I)alamin intermediate of the cobalamin-dependent methionine synthase (MetH). QM(DFT)/MM calculations on the methylcobalamin (MeCbl) binding domain of MetH reveal that the transfer of the methyl group to the substrate is associated with the displacement of the histidine axial base (His759). The axial base oscillates between a His-on form in the Me-cob(III)lamin:MetH resting state, where the Co—N(His759) distance is 2.27 Å, and a His-off form in the cob(I)alamin:MetH intermediate (2.78 Å). Furthermore, QM/MM and gas phase DFT calculations based on an unrestricted formalism show that the cob(I)alamin intermediate exhibits a complex electronic structure, intermediate between the Co(I) and Co(II)-radical corrin states. To understand this complexity, the electronic structure of $\text{Im} \cdots [\text{Cob(I)alamin}]$ is investigated using multireference CASSCF/QDPT2 calculations on gas phase models where the axial histidine is modeled by imidazole (Im). It is found that the correlated ground state wave function consists of a closed-shell $\text{Co}^{\text{I}} (\text{d}^8)$ configuration and a diradical contribution, which can be described as a $\text{Co}^{\text{II}} (\text{d}^7)$ -radical corrin (π^*)¹ configuration. Moreover, the contribution of these two configurations depends on the Co—N_{Im} distance. At short Co—N_{Im} distances (<2.5 Å), the dominant electronic configuration is the diradical state, while for longer distances it is the closed-shell state. The implications of this finding are discussed in the context of the methyl transfer reaction between the Me-H₄folate substrate and cob(I)alamin.

1. INTRODUCTION

The key step in the catalytic cycle of the cobalamin-dependent methionine synthase (MetH) enzyme is the transfer of a methyl group from the methylcobalamin (MeCbl) cofactor to the homocysteine (Hcy) substrate.^{1–14} The resulting cob(I)alamin intermediate is remethylated by methyl-tetrahydrofolate (Me-H₄folate) to generate back methyl-cob(III)alamin and tetrahydrofolate (H₄folate; Scheme 1).^{15–19} In other words, during the catalytic cycle, the cobalt center oscillates between methyl-cob(III)alamin and cob(I)alamin.

The MetH enzyme has a modular architecture, and the catalytic methyl transfer involves the interaction among different domains.²⁰ The crystal structure of the whole enzyme has not yet been resolved, mainly owing to the very high degree of conformational flexibility, but the X-ray crystal structure of individual domains,^{18,21–23} including the one that binds MeCbl,¹⁵ has been well characterized. During the course of catalytic reaction (Scheme 1), the two domains binding the MeCbl cofactor and the Hcy substrate form a reaction complex in which the substrate interacts with the MeCbl from the upper face of the cofactor. However, there is no structural information available with regard to the reaction complex, and therefore, the details of the reaction mechanism involving methylation

of the Hcy substrate remain a subject of debate. It is generally believed that the enzyme operates via an $S_{\text{N}}2$ -type nucleophilic displacement,^{7,8} though an alternative mechanism in which the one-electron reduction of the MeCbl cofactor takes place has also been proposed.^{24,25} This pathway does not impose specific geometrical and distance constraints with respect to the substrate and cofactor as does the $S_{\text{N}}2$ mechanism, which may be advantageous from the enzymatic point of view.

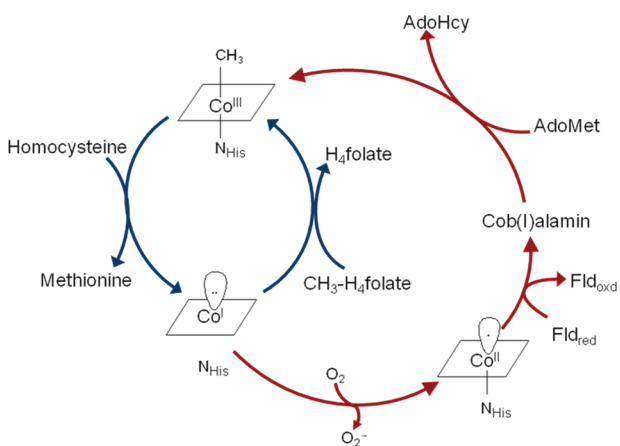
The transfer of the methyl group from the MeCbl cofactor to the Hcy substrate results in the formation of the cob(I)alamin intermediate.^{26,27} In solution, this complex is tetra-coordinated because the change of the Co oxidation state induces the detachment of the axial 5,6-dimethylbenzimidazole (DBI) base (Figure 1a).²⁸ However, the question is how such displacement of the axial His base takes place inside the enzyme. Due to its high reactivity, there are no structural data available for the enzyme-bound cob(I)alamin.

Several theoretical studies have investigated the electronic and structural properties of the tetra-coordinated cob(I)alamin complex (i.e., without the axial base) using density functional theory

Received: January 27, 2011

Published: April 14, 2011

Scheme 1. The Catalytic Cycle (Shown in Blue) and the Reactivation Cycle (Shown in Red) for the Cobalamin-Dependent Methionine Synthase (MetH)^a



^a H₄folate, tetrahydrofolate; CH₃-H₄folate, methyl-tetrahydrofolate; Fld_{oxd}, oxidized form of flavodoxin; Fld_{red}, reduced form of flavodoxin; AdoHcy, adenosyl-homocysteine; AdoMet, adenosyl-methionine.

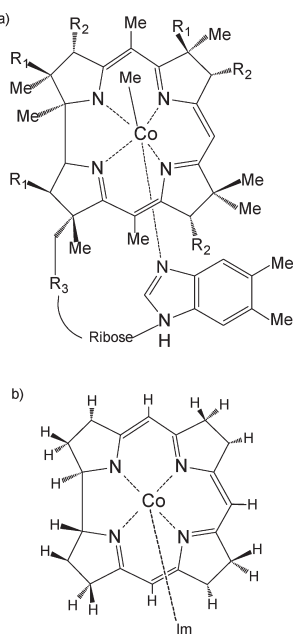


Figure 1. (a) Molecular structure of free methylcobalamin, where R = CH₃, R₁ = CH₂CONH₂, R₂ = CH₂CH₂CONH₂, and R₃ = (CH₂)₂CONHCH₂CH(CH₃)OPO₃. (b) Gas phase model of the Im...[Cob(I)alamin] enzymatic intermediate employed in the present work.

(DFT) as well as multireference CASSCF calculations.^{29–32} Jensen and Ryde³⁰ first noticed that the B3LYP-based wave function of the ground-state has a singlet instability, indicative of a complex wave function involving other configurations than Co^I(d⁸). Later, Jensen³¹ demonstrated that the ground state of cob(I)alamin is multiconfigurational using CASSCF/CASPT2 calculations. The correlated wave function was found to consist of a closed-shell Co^I(d⁸) configuration (67%) and a diradical Co^{II}(d⁷)-radical corrin (π^*)¹ configuration (23%). The formation of such unusual electronic configuration was explained by the overlap of low-lying metal d

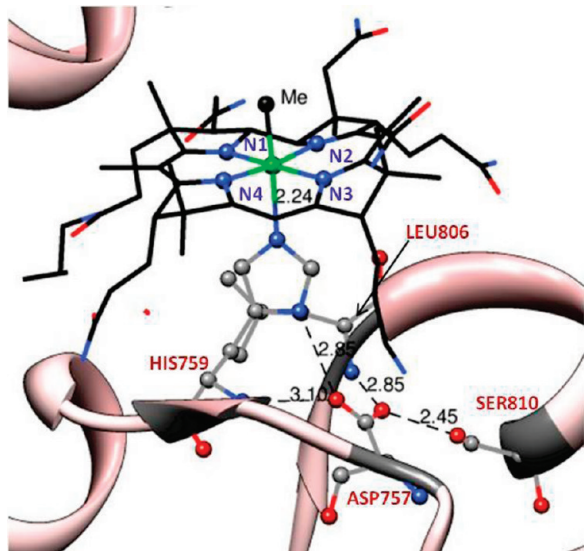


Figure 2. Close view of active site of MeCbl in the enzyme showing the interaction of lower axial ligand His759 with the other residues of the triad (Asp759, Ser810) as well as the nearby Leu806 based on the 1BMT crystal structure.¹⁵

orbitals with ligand orbitals at the singlet ground state, allowing the transfer of an electron from the Co to the corrin ligand. In this regard, the electronic structure of cob(I)alamin resembles the heme-based compound I intermediates, as pointed out by Ryde and Jensen.³³ Both cofactors have a noninnocent macrocycle that can exchange electrons with the metal. In compound I, one electron is transferred from the porphyrin to the Fe metal atom, whereas in the case of cob(I)alamin, electron transfer takes place in the opposite direction, i.e., from Co to the corrin ligand. Indeed, this proposed electron transfer is in agreement with a previous TD-DFT(B3LYP) study by Jaworska and Ladowski,²⁹ who found that the lowest energy bands (at 700 and 554 nm) in the electronic absorption spectrum of cob(I)alamin have d → π^* metal-to-ligand charge transfer (MLCT) character. However, a subsequent TD-DFT(PBE) study by Liptak and Brunold³² questioned the open-shell antiferromagnetic contribution to the ground state. As will be shown later, the use of a nonhybrid DFT functional is probably the cause of this discrepancy.

Nevertheless, all of those studies were carried out for isolated models of cob(I)alamin without the presence of the axial base or inclusion of the enzymatic environment. Therefore, the actual coordination number and electronic structure of the cob(I)alamin intermediate in MetH remain an open subject. During the catalytic methyl transfer reaction (Scheme 1), different enzyme domains interact with each other in order to either cleave or generate the Co–C bond. Simultaneously, the His759 residue is expected to move with respect to the Co metal center to break/form the Co–N_{His759} bond by analogy with the solution chemistry of the B₁₂ cofactor.²⁸ However, the crystal structure of the Me-cob(III)lamin resting state¹⁵ (PDB code: 1BMT, 3 Å resolution) shows that His759 interacts with Asp757 and Ser810 through a network of hydrogen bonds, suggesting that His759 would be fixed with respect to the Co center (Figure 2). On the other hand, a structural study of the reactivation complex²² (Scheme 1) formed by the adenosyl–methionine (AdoMet) and cob(I)alamin binding domains shows that the axial His759 moves away from the cobalt center and makes specific contacts with the AdoMet domain. Thus, it is still ambiguous

how His759 interacts with the cob(I)alamin cofactor during the catalytic cycle.

The purpose of this study is two-fold: First, the coordination of the axial His759 and the cob(I)alamin cofactor inside the enzyme is explored by employing the QM/MM approach. Second, the complex electronic structure of the cob(I)alamin intermediate suggested by the QM/MM results is analyzed using DFT and CASSCF/QDPT2 calculations on gas phase models. Finally, the implications of this finding are discussed in the context of the methyl transfer reaction between the Me-H₄folate and cob(I)alamin.

2. COMPUTATIONAL DETAILS

Three different theoretical methods were used to study the cob(I)alamin intermediate. First, the formation of the Co(I) state was investigated inside the cobalamin-dependent methionine synthase (MetH) enzyme employing QM(DFT)/MM. Second, the complex electronic properties of the cob(I)alamin and the influence of the axial base were investigated using gas phase DFT calculations. Finally, the multiconfigurational character of the Im \cdots [Cob(I)alamin] was further analyzed using CASSCF/MC-XQDPT2 calculations.

2.1. QM(DFT)/MM Calculations. The crystal structure of the McB_I binding module of MetH (PDB code: 1BMT, at 3 Å resolution)¹⁵ was used to model the cob(I)alamin intermediate, by removing the methyl ligand and adjusting the number of electrons of the QM system, consistent with the Co(I) oxidation state. Initially, the His759 residue is bound to the Co center, since the starting crystal structure corresponds to the Me-cob(III)lamin resting state. However, upon QM/MM geometry optimization, the axial base is observed to detach from the Co(I) center. The hybrid QM(DFT)/MM calculations were performed using the method developed by Laio et al.,³⁴ which combines the first-principles MD method of Car and Parrinello³⁵ with a force-field MD methodology (i.e., QM/MM CPMD). All details regarding the QM/MM calculations can be found in ref 25. In short, the geometry of the cob(I)alamin intermediate was optimized as a closed-shell singlet using the BP86 functional,^{36,37} a plane wave basis set with a 70–90 Ry kinetic energy cutoff, and Martins–Troullier pseudopotentials³⁸ to describe the interaction between the ionic cores and the valence electrons. Two pseudopotentials were tested for the cobalt atom: one with nine valence electrons supplemented with nonlinear core corrections³⁹ and another with 17 valence electrons. To explore the possibility of spin polarization between the cobalt and the corrin, a single point calculation within the local spin density approximation (LSD) was also performed. Finally, since the GGA BP86 functional is suspected to have problems describing a possible open-shell singlet state in cob(I)alamin,^{30,31} the B3LYP functional was also tested.

2.2. Gas Phase DFT Calculations. To get further insight into the complex electronic properties of the cob(I)alamin intermediate suggested by the QM/MM calculations, we carried out gas phase calculations. First, we studied the His-off form of cob(I)alamin for comparison with previous studies.^{29–32} Two different gas phase models were used: a big model containing the full cofactor with all of the side chains and a truncated model with C₂ symmetry where the side chains have been replaced by hydrogen atoms. Second, we investigated the influence of the axial His759 in the electronic properties of cob(I)alamin. An imidazole (Im) molecule modeling the axial His759 was placed under the Co center in accordance with the orientation obtained

from the QM/MM calculations, and a series of displacements along the Co(I)–N_{Im} coordinate was generated. Geometry optimization of all models was carried out employing the Becke–Perdew (BP86)^{36,37} functional and the 6-31G(d) (5d components) basis set, as implemented in Gaussian 03.⁴⁰ This level of theory constitutes an appropriate platform for describing the structural and electronic properties analysis of alkyl-cobalt(III) complexes, as documented in the literature.^{41–43} However, pure GGA functionals such as PBE⁴⁴ or BP86 are known to be unable to converge to a spin polarized solution for Co(I) complexes.^{30,31} This is not the case for hybrid functionals such as B3LYP, despite the fact that this functional underestimates the strength of the Co–C bond.^{45,46} Therefore, we used B3LYP to test the possibility of a spin-polarized solution, which may be indicative of a more complex electronic wave function.⁴⁷ In particular, B3LYP calculations were initially performed on all models having an even number of electrons, assuming a singlet closed-shell wave function. Then, the unrestricted Kohn–Sham formalism using UB3LYP was applied by mixing HOMO and LUMO orbitals to obtain the corresponding open-shell singlet. For each broken-symmetry solution, we examined the extent of spin polarization between the cobalt and the corrin by analyzing the spin density distributions.

2.3. CASSCF/MC-XQDPT2 Calculations. Since the Kohn–Sham formalism (which is the base for DFT-based computations) is restricted to a single Slater determinant description, it cannot describe the multiconfigurational character of the cob(I)alamin system. Thus, we carried out CASSCF multireference calculations, followed by quasi-degenerate perturbation theory (QDPT2)⁴⁸ calculations with a multiconfigurational self-consistent-field reference function (MC-XQDPT2) to include the dynamical correlation, as implemented in the PC GAMESS/Firefly QC package.⁴⁹ All of the CASSCF calculations were performed on the DFT optimized structures of the cob(I)alamin models (without and with the Im base) using the 6-31G(d) basis set. The details regarding the active space chosen for these multireference calculations are described in section 3.3.

3. RESULTS AND DISCUSSION

3.1. Structure of Cob(I)alamin Inside Meth. MetH is a modular enzyme composed of four functional domains.²⁰ The one considered here is the McB_I binding module,¹⁵ in which the His759 side chain serves as the lower axial ligand (Figure 2), instead of the DBI base of the free McB_I cofactor (Figure 1a). During the course of enzymatic methyl transfer, the cobalt center oscillates between the Co(III) and the Co(I) oxidation states, and the axial His is expected to dissociate from the cobalt center by similarity with the behavior of the B₁₂ cofactor in solution. However, this assumption remains to be proved since the crystal structure of the cob(I)alamin intermediate is not available. Here, we have investigated the coordination of the axial His759 and the cob(I)alamin in the MetH enzyme by means of QM/MM calculations.

The QM/MM optimized structure of the cob(I)alamin:MetH intermediate is shown in Figure 3, and the main structural parameters are listed in Table 1. The optimized structure of the Me-cob(III)lamin:MetH resting state²⁵ is also included for comparison. The fact that the X-ray Co–N_{ax} bond length for Me-cob(III)alamin:MetH is very well reproduced at the QM/MM level strengthens our confidence that the demethylated cob(I)alamin:MetH form would also be well characterized from

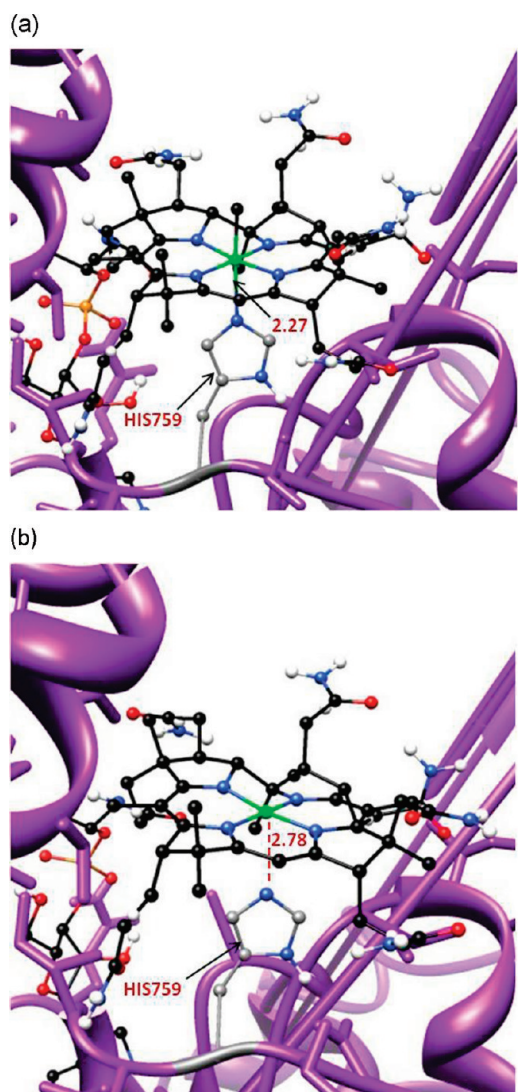


Figure 3. QM(DFT)/MM optimized structures of MeCbl binding domain of the MetH (a) hexa-coordinated Me-Cob(III)alamin resting state and (b) Cob(I)alamin intermediate.

Table 1. Key Structural Parameters of the Cofactor Binding Domain of MetH in the Me-Cob(III)alamin Resting State (MeCbl:MetH) and the Cob(I)alamin Intermediate (Co(I):MetH)^a

parameter	MeCbl:MetH		Co(I):MetH
	QM/MM ²⁵	X-ray ¹⁵	QM/MM ^b
Co–C	1.99	1.96	
Co–N _{Im}	2.27	2.24	2.78
Co–N1	1.88	1.91	1.84
Co–N2	1.86	1.93	1.81
Co–N3	1.93	2.02	1.91
Co–N4	1.92	2.02	1.87

^a All distances are given in Å. ^b This work.

a structural point of view using the same level of theory (i.e., the BP86 functional). The calculations show that the Co–N_{ax}(His759) distance increases from 2.27 Å in the Co(III)

oxidation state to 2.78 Å for Co(I). In other words, the axial ligand is displaced due to the change of the Co oxidation state. This is in agreement with the X-ray absorption spectroscopic studies showing that cob(I)alamin in solution is not axially coordinated.²⁸

Nevertheless, it should be noted that, differently from the cofactor in solution, the Co atom inside the enzyme remains weakly coordinated to the His. Most likely the axial His in MetH cannot move away further from the Co because it is hydrogen-bonded to Asp757 (Figure 2). Both His759 and Asp757 residues are in a loop, conferring to them a certain degree of flexibility that allows the axial base to be displaced during the catalytic cycle without breaking the hydrogen bond between them. However, this flexibility is not unlimited, because Asp757 is also interacting with a serine of an α helix (Ser810) and a leucine of a β sheet (Leu806), and these secondary structures are not as flexible as the loop. As a consequence, the Co \cdots N(His) cannot increase beyond \sim 2.8 Å without disrupting this hydrogen bond network, something that probably has a high energy cost. Maintaining a weak Co(I)–His coordination may be advantageous from the enzymatic point of view, since it would allow the axial His to recoordinate easily to the cobalt center when the cofactor is remethylated. The His–Asp–Ser triad is expected to play a key role in the Co(I) remethylation reaction by modulating the interaction between the Co and the axial base. Interestingly, the His–Asp–Ser triad is conserved in all corrinoid-based proteins catalyzing methyl transfer reactions (except in an iron–sulfur corrinoid protein), and thus it is tempting to suggest that the triad plays a similar role in all of the members of this protein family. Indeed, Hegemeier et al.⁵⁰ draw a similar conclusion for another cobalamin-dependent enzyme, i.e., the methanol–cobalamin methyltransferase (MetABC), on the basis of the long Co–N distance (2.51 Å) observed in the crystal structure of the cob(I)amide intermediate and the methylation rate of Co(I) being completely dependent on the presence of the axial base.

The structure of the cob(I)alamin:MetH intermediate was initially optimized considering a closed-shell singlet electronic configuration. However, since previous DFT as well as CASSCF calculations^{29–32} have shown that free cob(I)alamin has a more complex electronic structure, we checked the possibility of having a spin polarized solution inside the enzyme by using the local spin density approximation. Despite several attempts, we were unable to converge the open-shell singlet either with BP86 or B3LYP. The obtained electronic state was found to be indeed an intermediate state between two electronic configurations: the closed-shell Co^I(d⁸) singlet and the open-shell Co^{II}(d⁷)-corrin radical (π^*)¹ singlet. The spin density distribution showed some unpaired electronic density on the cobalt and the corrin ring with opposite signs, i.e., some diradical character. Moreover, the total integrated absolute value of the spin density was 1 e⁻ (intermediate between the 0 unpaired electrons expected for a pure closed-shell singlet and the two unpaired electrons for an open-shell singlet). This suggests that the closed-shell and the open-shell singlet states are very close in energy, so unless we force the system to be a closed-shell singlet, the single-determinantal DFT calculations give an intermediate state between Co(I) and Co(II)-corrin radical.

In summary, our QM/MM calculations confirm the early proposal of Wirt et al.²⁸ that the axial His ligand oscillates between the His-on form in the Me-cob(III)alamin:MetH resting state (Co–N(His) distance = 2.27 Å) and the His-off form in the cob(I)alamin:MetH intermediate (2.78 Å). Such movement of His759 in the enzymatic environment is due to the changes in

the electronic structure at the metal center, i.e., from Co(III) to an intermediate Co(I)/Co(II) state. Hereafter, the complex electronic structure of the cob(I)alamin intermediate as well as the changes associated with the displacement of the axial base are further analyzed using DFT and CASSCF/QDPT2.

3.2. Structural and Electronic Analysis Based on DFT Calculations. 3.2.1. *His-off Cob(I)alamin Intermediate.* Table 2 shows the main structural parameters obtained for the gas phase models of the His-off form of the cob(I)alamin intermediate employing both the BP86 and B3LYP functionals. The geometries do not differ significantly from the one inside the MetH enzyme (Table 1), regardless of the model employed for the

Table 2. Main Structural Parameters of the Full and Truncated Cob(I)alamin Gas Phase Models^a

model	full			truncated			
	B3LYP ^b	BP86 ^b	PBE ³²	B3LYP ^b	BP86 ^b	PBE ³²	
parameter						CASSCF ³¹	
fold angle ⁶¹				6.2	6.9	7.3	6.1
Co—N1	1.84	1.82	1.83	1.84	1.83	1.84	1.85
Co—N2	1.85	1.83	1.85	1.84	1.83	1.84	1.85
Co—N3	1.91	1.90	1.92	1.91	1.89	1.91	1.91
Co—N4	1.90	1.89	1.90	1.91	1.89	1.91	1.91

^a All distances are given in Å, and angles are in deg. N1–N4 refers to the corrin nitrogen atoms. ^b This work.

cofactor (full model with all of the side chains or truncated model with C2 symmetry) or the functional used. In particular, the calculated Co—N_{eq} distances (1.82–1.85 Å) are in agreement with the average experimental value obtained from EXAFS studies (1.86–1.88 Å).²⁸

As for the electronic structure, the main difference between the two functionals is that only B3LYP gives a spin polarized solution. This may reflect that the nonhybrid functionals such as BP86 do not describe correctly the spin polarization,^{51,52} even though they give correct Co—C bond dissociation energies (BDE).⁴⁵ Figure 4 shows the (B3LYP) spin density distribution along with the number of unpaired electrons. There is one unpaired electron on the cobalt atom coupled antiferromagnetically with an unpaired electron on the corrin ring, consistent with a Co^{II}(d⁷)-corrin radical (π^*)¹ diradical state. The spin density distributions of the full (Figure 4a) and the truncated (Figure 4b) models are almost identical. The side chains do not show any spin density, and the density exhibits 2-fold symmetry. Consequently, the truncated model with C2 symmetry was used for further analysis (Figure 4b).

From the energetic point of view, the open-shell singlet was found to be \sim 4 kcal/mol (B3LYP) lower in energy than the corresponding closed-shell configuration. Moreover, the ferromagnetic counterpart of the open-shell singlet, a triplet Co^{II}(d⁷)-radical corrin (π^*)¹ state, was also found to be 3 kcal/mol lower in energy than the closed-shell singlet, further validating the diradical contribution to the cob(I)alamin intermediate. Although these small energy differences are

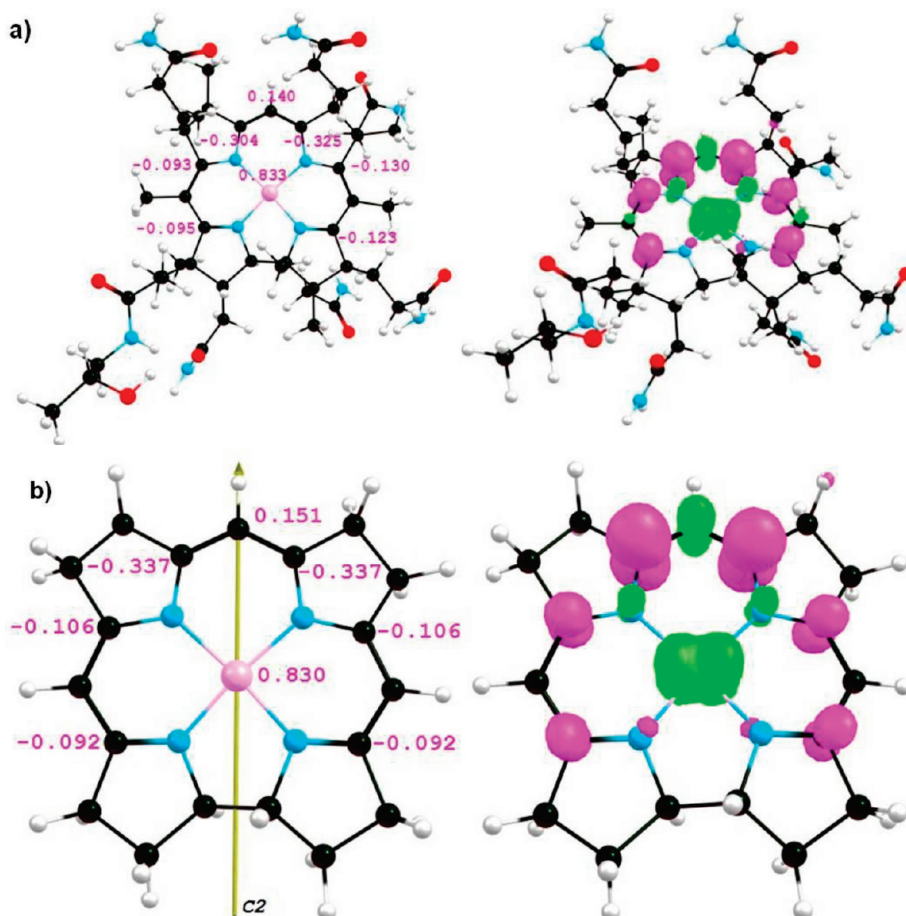


Figure 4. Spin density of (a) the full cob(I)alamin model and (b) the truncated cob(I)alamin model with C2 symmetry, computed at the B3LYP/6-31G(d) 5d level of theory. Left, spin populations; right, α and β spin density distributions colored as green and magenta, respectively.

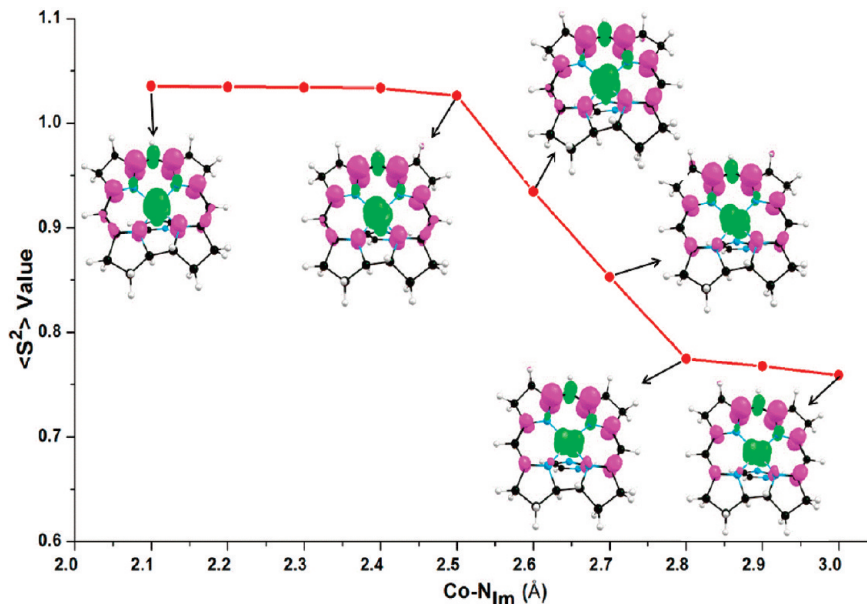


Figure 5. Evolution of the expectation value of the total spin, $\langle S^2 \rangle$, along with the spin density distributions during the elongation of the Co–N_{Im} distance in the Im...[Cob(I)alamin] model system.

within the error of the B3LYP calculation, they indicate that the closed-shell and the diradical states are close in energy, thus suggesting that the electron transfer from the Co^I(d⁸) to the corrin(π) to originate the Co^{II}(d⁷)-corrin radical(π^*)¹ may be feasible (see section 3.3).

3.2.2. Influence of the Axial Base His. The electronic properties of cob(I)alamin were also evaluated in the presence of an imidazole (Im) as a model of the His axial base. Since the His759 moves between 2.27 and 2.78 Å with respect to the Co center inside the enzyme, the Co(I)–N_{Im} distance was systematically varied between 2.1 and 2.8 Å in the gas phase DFT calculations. For each Co–N_{Im} distance, the structure was optimized with both the BP86 and the B3LYP functionals. As for the His-off model (section 3.2.1), the structure does not differ significantly between the two functionals, but a spin polarized solution was only obtained in the case of the B3LYP functional.

The spin density profiles (Figure 5 and Figure S1, Supporting Information) show unpaired spin density on the Co and the corrin ring, with opposite signs, consistent with a Co^{II}(d⁷)-corrin radical (π^*)¹ diradical state. However, it should be noted that the expectation value of the total spin $\langle S^2 \rangle$ is much larger (1.05–0.75) than the value expected for a singlet, $S(S + 1) = 0$, indicating that the open-shell singlet is significantly contaminated by the triplet state. Therefore, the single-determinantal DFT results need to be interpreted with caution. Nevertheless, we believe that the analysis of $\langle S^2 \rangle$ with respect to the Co–N_{Im} distance (Figure 5) could help to assess the extent of the diradical character. The initial $\langle S^2 \rangle \sim 1.05$ value remains constant until the distance reaches ~ 2.5 Å and decreases up to $\langle S^2 \rangle \sim 0.75$ at longer distances. This could indicate a decrease in the mixing between the open-shell singlet and triplet states due to an increase in the energy gap between them (see below).

Interestingly, the change in $\langle S^2 \rangle$ is accompanied by a change in the symmetry of spin density distribution on the cobalt atom. This switch in the d orbital of the cobalt atom bearing the unpaired electron can be further explained by analysis of the energies of relevant molecular orbitals near the HOMO/LUMO

gap as a function of the Co–N_{Im} distance (Figure 6). The antiferromagnetic coupling occurs between the upper occupied orbital of the corrin (π^*_{corr}) and the singly occupied d orbital of the cobalt (d_{Co}). This d_{Co} orbital is the d_{z^2} orbital at short Co–N_{Im} distances, but it is the d_{yz} orbital at long distances, in agreement with the $d_{yz} \rightarrow \pi^*$ MLCT band observed in a previous study of the cob(I)alamin intermediate without the axial base.³¹ Moreover, the energy gap between the π^*_{corr} and the d_{Co} orbitals increases with the Co–N_{Im} distance, further supporting our previous suggestion that the energy gap between the open-shell singlet and the triplet states increases with the Co–N_{Im} distance.

In summary, the DFT calculations suggest that the cob(I)alamin intermediate has significant diradical character. They also indicate that the axial base modulates the nature of the coupling associated with Co^{II}(d⁷)-corrin radical (π^*)¹ configuration by changing the energy of the d orbitals of the cobalt atom. However, the multiconfigurational character of the cob(I)alamin can only be assessed correctly using a multireference method.

3.3. CASSCF/MC-XQDPT2 Analysis. The multiconfigurational nature of the wave function of cob(I)alamin was further investigated using multireference methods (CASSCF and CASSCF/MC-QDPT2). The selection of active orbitals for complex systems such as cob(I)alamin always represents a challenging problem. Using previously reported CASSCF calculations on corrin^{31,53–55} or corrol-based⁵⁶ complexes as a guide, we have examined several kinds of active spaces and finally chosen to use a space of 10 active electrons distributed in 11 active orbitals.

Initially, CASSCF(10,11) calculations were carried out for the His-off form of cob(I)alamin (truncated model with C₂ symmetry, see section 3.2.1.) in order to reproduce the weight of the diradical contribution reported by Jensen.³¹ The active space, as shown in Figure S2 (Supporting Information), is very similar to that reported in ref 31. Second, we probed the effect exerted by the axial ligand on the electronic structure of the Im...[Co^I-(corrin)] complex by performing a series of different CASSCF calculations with the same active space (Figures 7 and Supporting Information, S3–S9) but varying the Co–N_{Im} distance

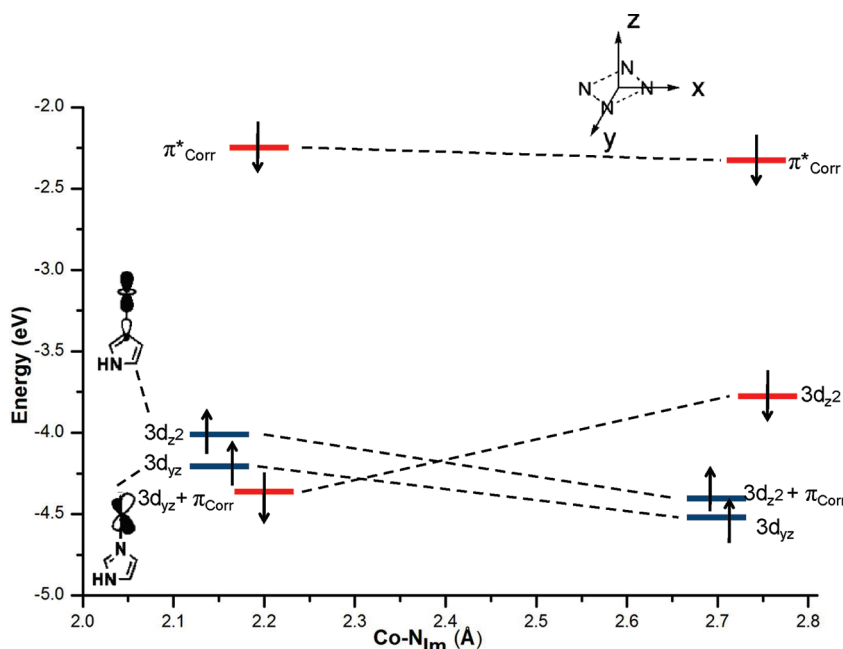


Figure 6. Variation of HOMO and HOMO–1 based orbital energies with the Co–N_{Im} distance calculated at the UB3LYP level of theory.

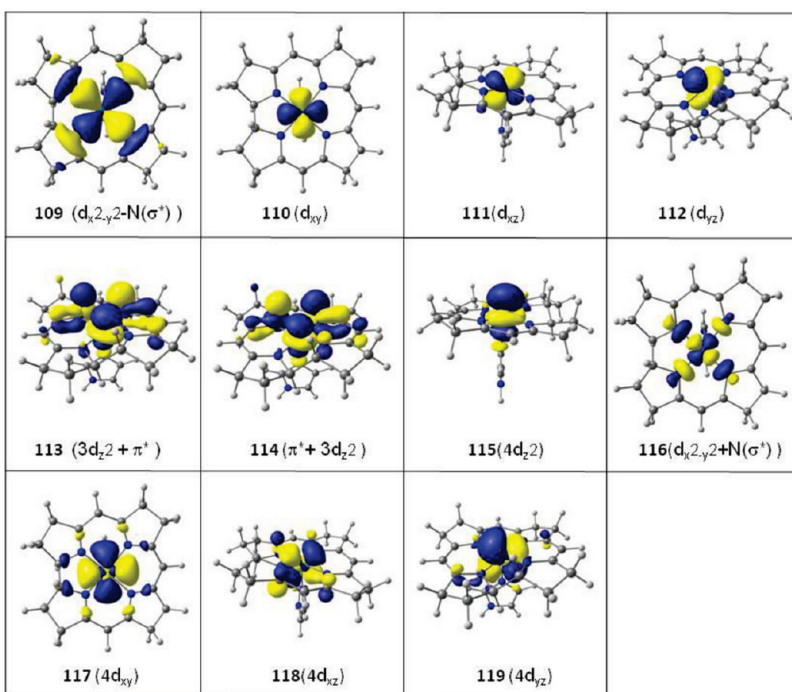


Figure 7. CASSCF active space orbitals used in the calculations of the Im···[Cob(I)alamin] model system at a Co–N_{Im} distance = 2.2 Å.

from 2.1 Å to 2.8 Å. In particular, the active space for Im···[Co^I(corrin)] is comprised of the $d_{x^2-y^2}-N(\sigma^*)$, d_{xy} , d_{xz} , d_{yz} , and $3d_{z^2} + \pi^*$ orbitals, and the respective correlating orbitals are $\pi^* + 3d_{z^2}$, $4d_{z^2}$, $d_{x^2-y^2} + N(\sigma^*)$, $4d_{xy}$, $4d_{xz}$, and $4d_{yz}$ (Figure 7). Note that this active space includes not only cobalt orbitals but also the corrin orbitals that may be important for the charge transfer between the corrin ring and the metal. The pair of correlating orbitals numbered 109 and 116 describe a σ^* donation from the lone electron pairs of the equatorial nitrogen atoms

to the $d_{x^2-y^2}$ orbital of cobalt. In addition, we have included the lowest unoccupied π^* orbital of corrin, because it has been shown to be necessary to describe the electron configuration of the His-off form of cob(I)alamin.³¹ This orbital mixes with the $3d_{z^2}$ cobalt orbital at a short Co–N_{Im} distance (CASSCF orbitals numbered 113 and 114, see Figure 7 and Figure S3–S5, Supporting Information), but with the $3d_{yz}$ orbital at long distances (CASSCF orbitals numbered 112 and 114, see Figures S6–S9, Supporting Information). Finally, an extra orbital has been added

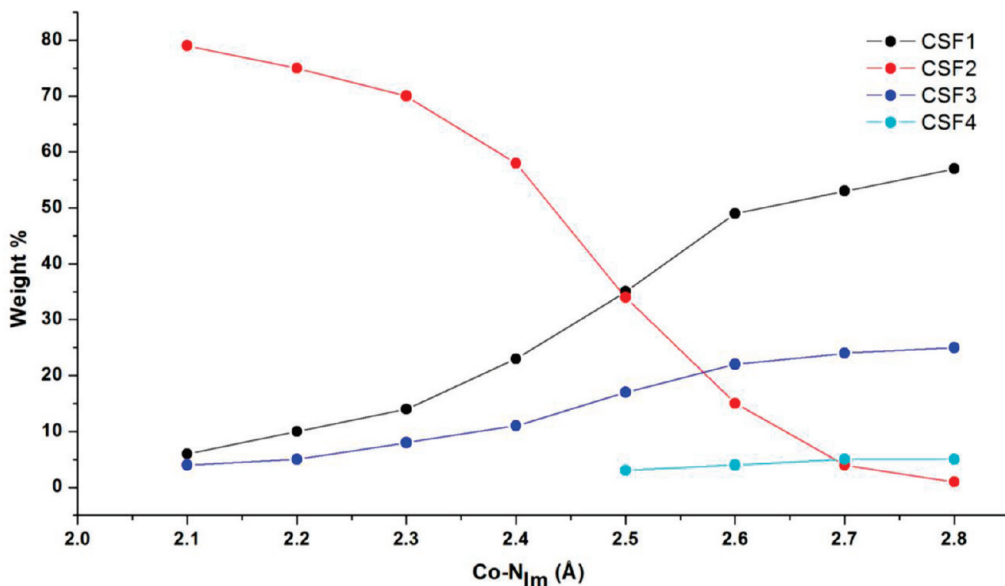


Figure 8. Weight (%) of the major configurations (CSFs) contributing to the ground state CASSCF wave function as a function of the Co–N_{Im} distance for the Im···[Cob(I)alamin] model system. The description of the CSFs is given in Table 3.

Table 3. Composition of the CASSCF Wave Function of Cob(I)alamin for Each Co–N_{Im} Distance, in Terms of the Mulliken Occupation Numbers of the Three Natural Orbitals Involved in the Open-Shell Singlet Description and the Weights of the Major Configurations State Functions (CSF1, CSF2, CSF3, and CSF4)

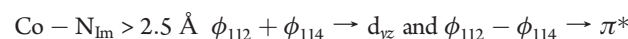
Co–N _{Im} (Å)	orbital occupation ^a	CSF1 (d _{z²}) ² (π*) ⁰ (wt %)	CSF2 (d _{z²}) ¹ (π*) ¹ (wt %)	CSF3 (d _{y^z}) ¹ (π*) ¹ (wt %)	CSF4 (d _{y^z}) ² (π*) ⁰ (wt %)
2.1	...(d _{y^z}) ^{1.97} (d _{z²}) ^{1.19} (π*) ^{0.81} ...	6	80	3	
2.2	...(d _{y^z}) ^{1.97} (d _{z²}) ^{1.21} (π*) ^{0.79} ...	10	76	6	
2.3	...(d _{y^z}) ^{1.97} (d _{z²}) ^{1.23} (π*) ^{0.76} ...	11	72	5	
2.4	...(d _{y^z}) ^{1.96} (d _{z²}) ^{1.34} (π*) ^{0.66} ...	19	60	8	
2.5	...(d _{y^z}) ^{1.90} (d _{z²}) ^{1.50} (π*) ^{0.57} ...	35	36	15	3
2.6	...(d _{y^z}) ^{1.50} (d _{z²}) ^{1.94} (π*) ^{0.51} ...	51	13	21	4
2.7	...(d _{y^z}) ^{1.59} (d _{z²}) ^{1.95} (π*) ^{0.42} ...	57	4	24	5
2.8	...(d _{y^z}) ^{1.59} (d _{z²}) ^{1.95} (π*) ^{0.42} ...	59	1	24	5

^a The Mulliken population analysis is shown for three natural orbitals involved in the open-shell singlet state. The rest of the active space orbitals are represented by dots.

to the correlating orbitals, in order to include the double shell effect⁵⁷ to all d orbitals.

The calculations reveal that the overall wave function of cob(I)alamin has multireference character, comprising five major configuration state functions (CSFs) that include single and double excitations (Figure S10, Supporting Information). By means of a unitary transformation to localized orbitals, this complex wave function can be simplified to four dominant configuration state functions (CSFs), as plotted in Figure 8. CSF1 is the closed-shell singlet, corresponding to the Co^I(d⁸)-corrin (π*)⁰ configuration. The open-shell singlet, representing the Co^{II}(d⁷)-corrin radical (π*)¹ configuration, consists of two major configurations (CSF2 and CSF3), both corresponding to charge transfer states where one electron from a d orbital of Co (d_{z²} or d_{y^z}, respectively) has been shifted to the corrin π* orbital. In addition, there is a small contribution of the double metal-to-ligand excitation, i.e., Co^{III}(d⁶)-corrin anion(π*)² (CSF4). Interestingly, the weight of these different CSFs varies with the Co–N_{Im} distance. The weight of the closed-shell Co^I(d⁸) configuration increases with the Co–N_{Im} distance, as the overall diradical character decreases. However, the behavior of the

two-diradical contributions is different. The weight of CSF2 decreases abruptly for Co–N_{Im} distances > 2.5 Å, whereas the weight of CSF3 increases. The crossing between the two diradical configurations takes place at ~2.6 Å and can be explored by analyzing the Mulliken populations (Table 3) and the pure fragment orbitals obtained after localization (Figure 9). When the Co–N_{Im} distance is shorter than 2.5 Å, the electron is transferring from the d_{z²} cobalt orbital to the corrin π* orbital, whereas when it is longer than 2.5 Å the electron is shifted from d_{y^z} to π*. Indeed, the localized orbitals are consistent with the orbitals resulting from adding and subtracting the original HOMO (or HOMO–1 for longer Co–N_{Im} distances) and LUMO orbitals for each Co–N_{Im} distance:



This switch in the cobalt d orbitals with the change in the axial bond length is consistent with the spin-polarized results obtained

from DFT(UB3LYP) calculations. The availability of different cobalt d orbitals in the active space chosen for the calculations allows the system to change the d_{Co} orbital that participates in the diradical state during the elongation of the Co–N_{Im} distance. It should also be noted that the overlap between the π^* corrin orbital and the singly occupied cobalt d orbital is larger for d_{yz} than for d_{z^2} , resulting in a higher weight for the CSF3 configuration than for CSF2, although the sum of both contributions reduces significantly with increasing Co–N_{Im} distance. This is in line with the increasing closed-shell character as well as the appearance of the small contribution from the double excitation (CSF4).

In addition, state average CASSCF/MC-XQDPT2 calculations also reveal that each excited state has a significant diradical character, showing metal-to-ligand charge transfer (Table S1, Supporting Information). Thus, at Co–N_{Im} = 2.1 Å, the correlated wave function of the ground state is mainly composed of the open-shell

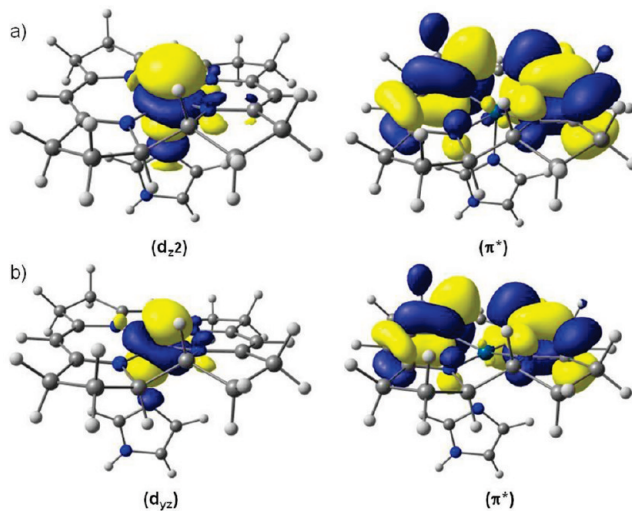


Figure 9. Pure fragment localized orbitals, describing the electron transfer between the cobalt and the corrin. (a) Co–N_{Im} distance < 2.5 Å; the electron is transferred from Co(d_{z²}) to corrin(π^*). (b) Co–N_{Im} distance > 2.5 Å; the electron is shifted from Co(d_{y_z}) to corrin(π^*).

singlet, Co^{II}(d⁷)-corrin radical (π^*)¹ configuration. This diradical weight decreases as the axial bond is elongated, such that at Co–N_{Im} = 2.8 Å the diradical weight is only 24%, similar to the result obtained by Jensen³¹ for the cob(I)alamin model without an axial base. In other words, the dominant contribution to the ground state wave function is the diradical configuration when the His is bound to the cobalt atom, but the closed-shell singlet, Co^I(d⁸) configuration when the axial His is weakly coordinated.

3.4. Energy Changes as Function of Co–N_{Im} Distance.

Finally, we have calculated the energy of the Im · · · [Co^I(corrin)] complex as a function of the distance between Co and N_{Im} atoms in order to evaluate the energy cost of displacing the axial ligand (Figure 10). We have employed single-determinant (DFT with either the BP86 or the B3LYP functional) and multireference (CASSCF and CASSCF/MC-XQDPT2) methods and different basis sets (6-31G(d) and 6-311G(d,p)). Regardless of the computational method used, the curve is clearly repulsive. However, it should be noted that the (CASSCF/MC-XQDPT2) energy at a Co–N_{Im} distance ~ 2.3 Å (i.e., in the Me-Cob-(III)alamin resting state of the MetH enzyme) is only 4 kcal/mol higher than at ~2.8 Å (i.e., the calculated value for the cob(I)alamin intermediate, see section 3.1). Therefore, although the change of distance causes noticeable changes in terms of electronic properties of the Co center (from Co^{II}-corrin radical to Co^I), it is energetically not costly.

3.5. Implications for the Remethylation of the Cob(I)alamin Intermediate in MetH. The methyl transfer reaction from Me-H₄folate to cob(I)alamin to generate the Me-cob(III)alamin resting state (Scheme 1) is generally assumed to occur through a S_N2-type displacement. However, in view of the present work, it can be suggested that (i) a radical mechanism, consisting of an electron transfer (ET) followed by a methyl radical transfer, is also possible and that (ii) the axial base would have a decisive role regarding the enhancement of the ET-based mechanism by modulating the cob(I)alamin electronic properties.

At shorter Co–N_{Im} distances (<2.5 Å), the dominant electronic configuration is diradical, with a Co(II) and an electron located on the corrin ring. This would favor the radical mechanism, in which an electron is initially transferred from the corrin to

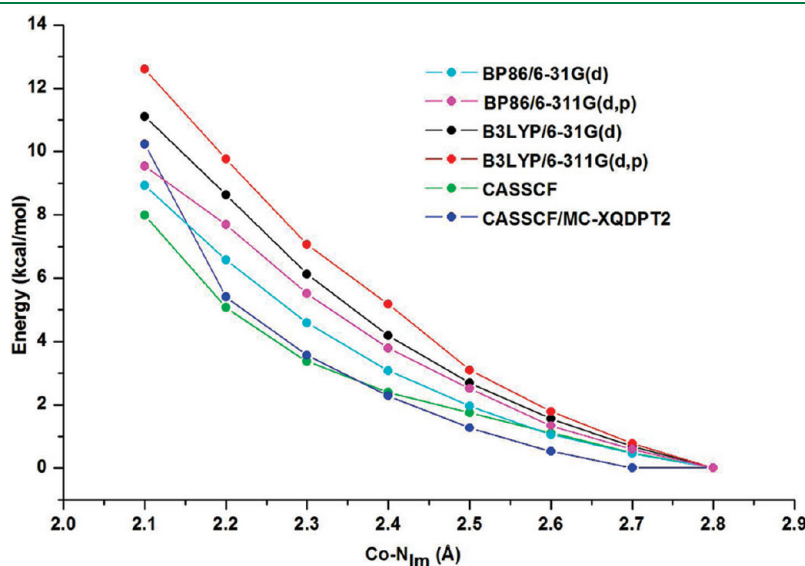


Figure 10. Change in the ground state energy with the Co–N_{Im} distance, computed with different DFT functionals and *ab initio* CASSCF/MC-XQDPT2 methods.

the Me-H₄folate in order to generate a Co(II) and [Me-H₄folate]^{•-} state. Subsequently, a methyl radical would be transferred from [Me-H₄folate]^{•-} to Co(II), forming Me-Cob(III)alamin. This methyl radical transfer would be in line with the reductive cleavage mechanism proposed for the methyl transfer from MeCbl to the Hcy substrate (Scheme 1), where the electron is transferred from the Hcy to the MeCbl, followed by a methyl radical transfer from the one electron reduced form of MeCbl to the Hcy substrate.^{24,25} In other words, the reaction mechanism of MetH would not only involve the Co metal but also the corrin ligand, which can activate both substrates (Me-H₄folate and Hcy) of the MetH enzyme by ET. On the other hand, at longer Co—N_{Im} distances (>2.5 Å), the dominant configuration is closed-shell, with an electron pair located on the metal center consistent with a Co(I) oxidation state. This would favor an S_N2-type mechanism in which the Co(I) nucleophile directly abstracts the methyl group of Me-H₄folate.

4. SUMMARY AND CONCLUSION

In the present theoretical study, the electronic and structural properties of the cob(I)alamin intermediate have been analyzed using QM(DFT)/MM, gas phase DFT, and CASSCF/QDPT2 calculations. Because previous studies^{29–32} did not take into account the influence of the protein environment, we initially performed QM/MM calculations to study the formation of the Co(I) state inside the MeCbl domain of the methionine synthase (MetH) enzyme. The observed displacement of the axial His759 from the cobalt center is in agreement with the model proposed by Wirt et al.²⁸ based on the tetracoordinated state of free cob(I)alamin. However, His759 is weakly coordinated inside the enzyme (QM/MM optimized Co—N(His) distance = 2.78 Å), where the presence of the catalytic triad (His759—Asp757—Ser810) and the hydrogen bonds with other residues reduce its conformational freedom. This implies that the remethylation of the cob(I)alamin cofactor by Me-H₄folate (Scheme 1) occurs in the presence of the axial ligand, and thus His759 may have an influence in this methyl transfer reaction.

Consequently, we have analyzed the influence of the axial ligand in the electronic structure of cob(I)alamin cofactor using gas phase DFT followed by CASSCF/QDPT2 calculations. Irrespective of the theoretical method used, our results show that the ground state of cob(I)alamin is multiconfigurational, in agreement with a previous study of the cob(I)alamin cofactor without the axial ligand.³¹ In addition to the closed-shell Co(I), a diradical Co(II)-corrin radical configuration (formed by electron transfer from the cobalt to the corrin ring) contributes to the electronic structure of the cob(I)alamin intermediate, revealing the noninnocent behavior of the corrin ring.³³ The weight of these two configurations depends on the distance of the axial base His from the Co center. The main contribution to the ground state wave function at short Co—N_{Im} distances is the diradical configuration, whereas at long distances, it is the closed-shell. Therefore, our results suggest that (i) the standard description of the Co(I) nucleophile is not appropriate for cob(I)alamin, due to the noninnocent character of the corrin ring, and (ii) the distance between cob(I)alamin and the axial His plays an important role in modulating the nucleophilicity of Co(I).

In view of our results, we have proposed that the remethylation reaction in MetH (Scheme 1) could involve not only the metal (i.e., the closed-shell Co(I) configuration) but also the corrin ring (i.e., the diradical Co(II)-corrin radical

configuration). In other words, in addition to the traditionally assumed S_N2 mechanism, our findings suggest the possibility of an alternative radical mechanism, in which an electron is transferred from the corrin to the Me-H₄folate in order to generate Co(II) and [Me-H₄folate]^{•-}. It should be noted that this ET does not require the presence of any strong reducing agent near the CH₃—H₄folate substrate but rather the cofactor-induced formation of anion-radical-like species within the cob(I)alamin:[Me-H₄folate] reactant complex. Indeed, earlier studies by Marcus,⁵⁸ Shaik et al.,⁵⁹ and Zipse⁶⁰ already discussed that such ET bond-breakage mechanisms significantly enhance the reaction rates in comparison to S_N2 mechanisms. The energetics and dichotomy of the S_N2 and radical mechanisms in the methyl transfer reaction from Me-H₄folate to cob(I)alamin are currently being investigated in our group.

■ ASSOCIATED CONTENT

S Supporting Information. Spin density distributions along with the spin populations of the Im^{•+}·[Cob(I)alamin] gas phase models, CASSCF active space orbitals of cob(I)alamin, CASSCF active space orbitals for the Im^{•+}·[Cob(I)alamin] model at Co—N_{Im} distances = 2.1–2.8 Å, major configurations contributing to the ground state CASSCF wave function before localization, relative energy of ground state and low lying excited states for each Co—N_{Im} distance, and Cartesian coordinates of the QM region of the QM/MM optimized structures of the cofactor binding domain of methionine synthase (MetH) in the Me-Cob(III)alamin and Cob(I)alamin intermediate. This material is available free of charge via the Internet at <http://pubs.acs.org>.

■ AUTHOR INFORMATION

Corresponding Author

*Phone: (502) 852-6609. Fax: (502) 852-8149. E-mail: pawel@louisville.edu.

■ ACKNOWLEDGMENT

N.K. and P.M.K. acknowledge the computer support and assistance provided by Cardinal Research Cluster Supercomputer Center at the University of Louisville. This work was also supported by the Ministry of Science and Higher Education (Poland) under grant no. N204 028336.

C.R. thanks the Spanish Ministry of Science and Innovation (MICINN, Grant FIS2008-03845) and the Generalitat de Catalunya (GENCAT, Grant 2009SGR-1309) for its financial assistance. M.A.-P. acknowledges an FI fellowship from GENCAT. C.R. and M.A.-P. also acknowledge the computer support, technical expertise, and assistance provided by the Barcelona Supercomputing Center—Centro Nacional de Supercomputación (BSC—CNS).

■ REFERENCES

- (1) Dolphin, D. *B₁₂*; Wiley-Interscience: New York, 1982.
- (2) Banerjee, R. *Chem. Biol.* 1997, 4, 175–186.
- (3) Ludwig, M. L.; Matthews, R. G. *Annu. Rev. Biochem.* 1997, 66, 269–313.
- (4) *Vitamin B₁₂ and B₁₂ Proteins*; Kräutler, B., Arigoni, B., Golding, B. T., Eds.; Wiley-VCH: New York, 1998 (Lectures Presented at the 4th European Symposium on Vitamin B₁₂ and B₁₂ Proteins).
- (5) Marzilli, L. G. In *Bioinorganic Catalysis*; Reedijk, J., Bouwman, E., Eds.; Marcel Dekker: New York, 1999; pp 423–468.

- (6) Banerjee, R. *Chemistry and Biochemistry of B12*; Wiley: New York, 1999.
- (7) Matthews, R. G. *Acc. Chem. Res.* **2001**, *34*, 681–689.
- (8) Banerjee, R.; Ragsdale, S. W. *Annu. Rev. Biochem.* **2003**, *72*, 209–247.
- (9) Brown, K. L. *Chem. Rev.* **2005**, *105*, 2075–2149.
- (10) Randaccio, L.; Geremia, S.; Nardin, G.; Wuerges, J. *Coord. Chem. Rev.* **2006**, *250*, 1332–1350.
- (11) Matthews, R. G.; Koutmos, M.; Datta, S. *Curr. Opin. Struct. Biol.* **2008**, *18*, 658–666.
- (12) Randaccio, L.; Geremia, S.; Demitri, N.; Wuerges, J. *Trends Inorg. Chem.* **2009**, *11*, 1–19.
- (13) Matthews, R. G. In *Metal Ions in Life Sciences*; Sigel, A., Sigel, H., Sigel, R. K. O., Eds.; Royal Society of Chemistry: Cambridge, U. K., 2009; Vol. 6, pp 53–114.
- (14) Randaccio, L.; Geremia, S.; Demitri, N.; Wuerges, J. *Molecules* **2010**, *15*, 3228–3259.
- (15) Drennan, C. L.; Huang, S.; Drummond, J. T.; Matthews, R. G.; Ludwig, M. L. *Science* **1994**, *266*, 1669–1674.
- (16) Goulding, C. W.; Matthews, R. G. *Biochemistry* **1997**, *36*, 15749–15757.
- (17) Pearisco, K.; Goulding, C. W.; Huang, S.; Matthews, R. G.; Panner-Hahn, J. E. *J. Am. Chem. Soc.* **1998**, *120*, 8410–8416.
- (18) Evans, J. C.; Huddler, D. P.; Hilgers, M. T.; Romanchuk, G.; Matthews, R. G.; Ludwig, M. L. *Proc. Natl. Acad. Sci. U. S. A.* **2004**, *101*, 3729–3736.
- (19) Koutmos, M.; Pejchal, R.; Bomer, T. M.; Matthews, R. G.; Smith, J. L.; Ludwig, M. L. *Proc. Natl. Acad. Sci. U. S. A.* **2008**, *105*, 3286–3291.
- (20) Goulding, C. W.; Postigo, D.; Matthews, R. G. *Biochemistry* **1997**, *36*, 8082–8091.
- (21) Dixon, M. M.; Huang, S.; Matthews, R. G.; Ludwig, M. *Structure* **1996**, *4*, 1263–1275.
- (22) Datta, S.; Koutmos, M.; Patridge, K. A.; Ludwig, M. L.; Matthews, R. G. *Proc. Natl. Acad. Sci. U. S. A.* **2008**, *105*, 4115–4120.
- (23) Bandarian, V.; Patridge, K. A.; Lennon, B. W.; Huddler, D. P.; Matthews, R. G.; Ludwig, M. L. *Nat. Struct. Biol.* **2002**, *9*, 53–56.
- (24) Kozlowski, P. M.; Kuta, J.; Galezowski, W. *J. Phys. Chem. B* **2007**, *111*, 7638–7645.
- (25) Alfonso-Prieto, M.; Biarnés, X.; Kumar, M.; Rovira, C.; Kozlowski, P. M. *J. Phys. Chem. B* **2010**, *114*, 12965–12971.
- (26) Lexa, D.; Saveant, J. M. *Acc. Chem. Res.* **1983**, *16*, 235–243.
- (27) Banerjee, R. V.; Frasca, V.; Ballou, D. P.; Matthews, R. G. *Biochemistry* **1990**, *29*, 11101.
- (28) Wirt, M. D.; Sagi, I.; Chance, M. R. *Biophys. J.* **1992**, *63*, 412–417.
- (29) Jaworska, M.; Lodowski, P. *THEOCHEM* **2003**, *631*, 209–223.
- (30) Jensen, K. P.; Ryde, U. *ChemBioChem* **2003**, *4*, 413–424.
- (31) Jensen, K. P. *J. Phys. Chem. B* **2005**, *109*, 10505–10512.
- (32) Liptak, M. D.; Brunold, T. C. *J. Am. Chem. Soc.* **2006**, *128*, 9144–9156.
- (33) Jensen, K. P.; Ryde, U. *Coord. Chem. Rev.* **2009**, *253*, 769–778.
- (34) Laiò, A.; Vandevondele, J.; Rothlisberger, U. *J. Chem. Phys.* **2002**, *116*, 6941–6947.
- (35) Car, R.; Parrinello, M. *Phys. Rev. Lett.* **1985**, *55*, 2471–2474.
- (36) Becke, A. D. *J. Chem. Phys.* **1986**, *84*, 4524–4529.
- (37) Perdew, J. P. *Phys. Rev. B* **1986**, *33*, 8822–8824.
- (38) Troullier, N.; Martins, J. L. *Phys. Rev. B* **1991**, *43*, 1993–2006.
- (39) Louie, S. G.; Froyen, S.; Cohen, M. L. *Phys. Rev. B* **1982**, *26*, 1738–1742.
- (40) Frisch, M. J.; Trucks, G. W.; Schlegel, H. B.; Scuseria, G. E.; Robb, M. A.; Cheeseman, J. R.; Montgomery, J. A., Jr.; Vreven, T.; Kudin, K. N.; Burant, J. C.; Millam, J. M.; Iyengar, S. S.; Tomasi, J.; Barone, V.; Mennucci, B.; Cossi, M.; Scalmani, G.; Rega, N.; Petersson, G. A.; Nakatsuji, H.; Hada, M.; Ehara, M.; Toyota, K.; Fukuda, R.; Hasegawa, J.; Ishida, M.; Nakajima, T.; Honda, Y.; Kitao, O.; Nakai, H.; Klene, M.; Li, X.; Knox, J. E.; Hratchian, H. P.; Cross, J. B.; Bakken, V.; Adamo, C.; Jaramillo, J.; Gomperts, R.; Stratmann, R. E.; Yazyev, O.; Austin, A. J.; Cammi, R.; Pomelli, C.; Ochterski, J. W.; Ayala, P. Y.; Morokuma, K.; Voth, G. A.; Salvador, P.; Dannenberg, J. J.; Zakrzewski, V. G.; Dapprich, S.; Daniels, A. D.; Strain, M. C.; Farkas, O.; Malick, D. K.; Rabuck, A. D.; Raghavachari, K.; Foresman, J. B.; Ortiz, J. V.; Cui, Q.; Baboul, A. G.; Clifford, S.; Cioslowski, J.; Stefanov, B. B.; Liu, G.; Liashenko, A.; Piskorz, P.; Komaromi, I.; Martin, R. L.; Fox, D. J.; Keith, T.; Al-Laham, M. A.; Peng, C. Y.; Nanayakkara, A.; Challacombe, M.; Gill, P. M. W.; Johnson, B.; Chen, W.; Wong, M. W.; Gonzalez, C.; Pople, J. A. *Gaussian 03*, revision C.02; Gaussian, Inc.: Wallingford, CT, 2004.
- (41) Rovira, C.; Kozlowski, P. M. *J. Phys. Chem. B* **2007**, *111*, 3251–3257.
- (42) Kuta, J.; Patchkovskii, S.; Zgierski, M. Z.; Kozlowski, P. M. *J. Comput. Chem.* **2006**, *27*, 1429–1437.
- (43) Kozlowski, P. M.; Kamachi, T.; Toraya, T.; Yoshizawa, T. *Angew. Chem., Int. Ed.* **2007**, *46*, 980–983.
- (44) Perdew, J. P.; Burke, K.; Ernzerhof, M. *Phys. Rev. Lett.* **1996**, *77*, 3865–3868.
- (45) Jensen, K.; Ryde, U. *J. Phys. Chem. A* **2003**, *107*, 7539–7545.
- (46) Ruiz, E.; Cirera, J.; Alvarez, S. *Coord. Chem. Rev.* **2005**, *249*, 2649–2660.
- (47) Becke, A. D. *J. Chem. Phys.* **1993**, *98*, 5648–5652.
- (48) Nakano, H. *J. Chem. Phys.* **1993**, *99*, 7983–7992.
- (49) Granovsky, A. A. PC GAMESS/Firefly version 7.1.G. www. http://classic.chem.msu.su/gran/gamess/index.html.
- (50) Hagemeier, C. H.; Kruer, M.; Thauer, R. K.; Warkentin, E.; Ermler, U. *Proc. Natl. Acad. Sci. U. S. A.* **2006**, *103*, 18917–18922.
- (51) Goel, S.; Masunov, A. E. *J. Chem. Phys.* **2008**, *129*, 214302–214316.
- (52) Jensen, K. P.; Roos, B. O.; Ryde, U. *J. Chem. Phys.* **2007**, *126*, 014103–014117.
- (53) Kozlowski, P. M.; Kamachi, T.; Kumar, M.; Nakayama, T.; Yoshizawa, K. *J. Phys. Chem. B* **2010**, *114*, 5928–5939.
- (54) Kornobis, K.; Kumar, N.; Wong, B. M.; Jaworska, M.; Lodowski P.; Andruniow, T.; Ruud, K.; Kozlowski, P. M. *J. Phys. Chem. A* **2011**, *115*, 1280–1292.
- (55) Kumar, N.; Jaworska, M.; Lodowski, P.; Kumar, M.; Kozlowski, P. M. *J. Phys. Chem. B* **2011**, doi:10.1021/jp200945a.
- (56) Roos, B. O.; Veryazov, V.; Conradie, J.; Taylor, P. R.; Ghosh, A. *J. Phys. Chem. B* **2008**, *112*, 14099–14102.
- (57) Roos, B. O.; Lindh, R.; Malmqvist, P.-Å.; Veryazov, V.; Widmark, P.-O. *J. Phys. Chem.* **2005**, *109*, 6575–6579.
- (58) Marcus, R. A. *J. Phys. Chem. A* **1997**, *101*, 4072–4087.
- (59) Shaik, S. S.; Schlegel, H. B.; Wolfe, S. *Theoretical Aspects of Physical Organic Chemistry. The SN2Mechanism*; Wiley-Interscience: New York, 1992.
- (60) Zipse, H. *Angew. Chem., Int. Ed. Engl.* **1997**, *36*, 1697–1700.
- (61) Rovira, C.; Biarnés, X. *Inorg. Chem.* **2004**, *43*, 6628–6632.